Refereed Proceedings

The 12th International Conference on Fluidization - New Horizons in Fluidization Engineering

Engineering Conferences International *Year* 2007

Laser Diagnostics of Hydrodynamics and Gas-Mixing in the Splash Zone of Gas-Fluidized Beds

Roberto Solimene* Antonio Marzocchella†

Raffaele Ragucci‡ Piero Salatino**

*Istituto di Ricerche sulla Combustione – CNR, rsolimen@unina.it

†Università degli Studi di Napoli Federico II

‡Istituto di Ricerche sulla Combustione – CNR

**Universita' degli Studi di Napoli Federico II, salatino@unina.it

LASER DIAGNOSTICS OF HYDRODYNAMICS AND GAS MIXING IN THE SPLASH ZONE OF GAS-FLUIDIZED BEDS

Roberto Solimene, Antonio Marzocchella, Raffaele Ragucci, Piero Salatino
Dipartimento di Ingegneria Chimica - Università degli studi di Napoli Federico II
Istituto di Ricerche sulla Combustione – CNR
Piazzale Tecchio, 80, 80125 Napoli Italy
T: +390817682258; F: +390815936936; E: salatino@unina.it

ABSTRACT

The hydrodynamic patterns of gas flow associated with bubbles bursting at the surface of gas-fluidized beds have been investigated by means of planar laser induced fluorescence using acetone as diffusive gas tracer. The flow structures generated by the eruption of an isolated bubble have been characterized as a function of bed material size and of bubble injection level.

INTRODUCTION

Gas mixing in the splash zone of fluidized beds affects the rate and yield of chemical processes when gas-phase chemical reactions take place under non-premixed or poorly-premixed conditions. This is, for instance, the case of fluidized bed combustors fuelled with high-volatile solid fuels (1-3): the rate of the fast gas-phase homogeneous volatile matter combustion is largely controlled by gas mixing in the splash zone of the combustor since devolatilization takes place at or near the bed surface. Similarly, the fate of fuel nitrogen in fluidized bed combustors, with specific reference to yield toward different nitrogen-bearing compounds, is largely controlled by gas mixing which, in combination with the intrinsic chemistry of nitrogen oxidation-reduction reactions, dictates the relevant conversion pathway (4).

Gas mixing in the splash zone is determined to a large extent by the hydrodynamics of bubble bursting at the surface of the fluidized bed. The “Pulsed Jet” or the “Ghost Bubbles” models have been advocated to represent hydrodynamics associated with bubble eruption. The former theory postulates that gas bubbles erupting at the bed surface behave as intermittent jets. Horio et al. (5) applied free-stream jet models to erupting bubbles to assess the decay of gas velocity along the jet centerline and the extent of gas entrainment. On the other hand, the “Ghost Bubbles” theory (6) assumes that the structure and the internal flow pattern of bubbles in the bed are largely retained in the freeboard upon bursting. Experimental studies (7-13) addressing the hydrodynamics of isolated bubble bursting at the bed surface show departures from both the pulsed jet and the ghost bubble theories. Flow characterization based on light scattering (7-11) or planar laser induced fluorescence (12) highlighted the formation of a downward vortex ring generated by the ejection/falling back of solids associated with bubble bursting. On the other hand, Pemberton and Davidson (6), using a hot wire anemometer, correlated time-resolved

The 12th International Conference on Fluidization - New Horizons in Fluidization Engineering, ART. 55 [2007]

heat transfer with the passage of the vortex ring whose kinematics was analyzed in the light of the ghost bubbles model. It is generally recognized that "turbulence" in the splash zone of a fluidized bed reactor is induced by bubble bursting at the bed surface. In particular, it is essentially related to jets associated with the eruption of coalescing bubbles at the bed surface or to bed surface oscillations. Crater-like radial profiles of axial velocity have been recognized as a typical feature of the hydrodynamics of the splash zone (7,14), a feature that could not easily be explained in the light of either the pulsed jet or the ghost bubbles theories.

The present paper addresses the hydrodynamic patterns associated with bubble bursting at the surface of gas fluidized beds by means of a flow visualization technique based on the planar laser induced fluorescence of acetone vapours. The present study extends previous work on the same subject (11,12) with the aim of assessing the effect of bed solids size (within the B group of the Geldart classification of powders) and the influence of the height of bed solids above the bubble injection level on hydrodynamic patterns associated with bubble bursting.

EXPERIMENTAL

Apparatus

The experimental apparatus, sketched in Fig. 1, consists of a fluidization column, a single bubble injector, a set of pressure transducers and a laser sheet source synchronized with a video camera recording system. The fluidization column is described elsewhere (11-12). The column is equipped with three flat quartz windows transparent to ultraviolet radiation and fitted to the wall of the column. The inset of Fig. 1 shows the relative position of the three windows: i) W1 and W2 (0.36 high and 0.03 m wide) enable the illumination of a planar domain located along one diameter; ii) W3 (0.36x0.10 m) enables the observation of the illuminated area inside the column. Traced bubbles are injected in the fluidization column by means of a 7 mm ID nozzle, mounted inside a 10 mm ID hole at the center of the gas distributor. The injector could be moved along the column centerline to vary the level at which bubbles were injected into the bed. Details on the injection device and on the procedure for the evaluation of the injected bubble size are reported elsewhere (11-12). The gas injected was bubbled in an acetone bath at 28°C prior to reaching the nozzle. The mole fraction of acetone in the traced gas was never smaller than 10 mol/m^3.

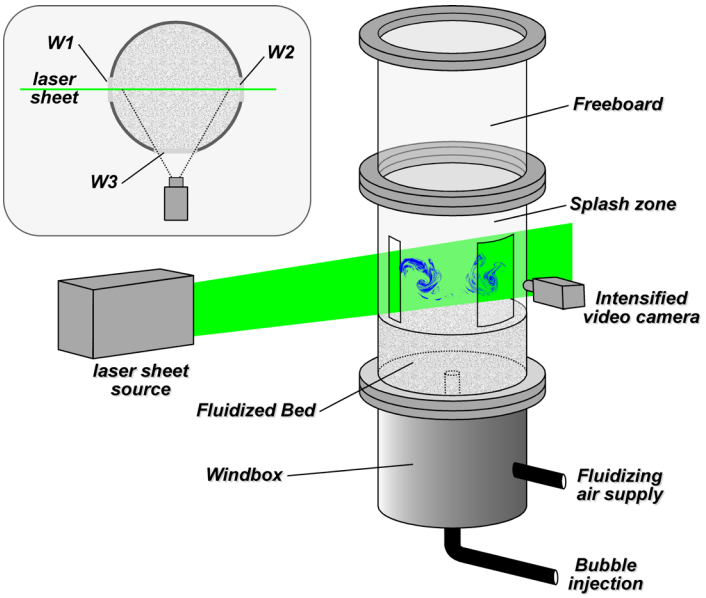

Fig. 1 The experimental apparatus. In the inset: a cross section of the fluidization column at the glass windows level (W1, W2 and W3).

Diagnostics

A Planar Laser Induced Fluorescence (PLIF) technique has been adopted. The light source

was a Nd:YAG pulsed laser whose fourth harmonic wavelength (at 266 nm) excited emission of the fluorescence signal from acetone. A Pellin-Broca prism, a cylindrical telescope and cylindrical lens were used to separate the desired laser harmonic, to shape the laser beam into a light sheet 1 mm thick and to enlarge the light sheet to fit a height of about 0.17 m. The light sheet crosses the fluidization column passing through the W1 and W2 window to illuminate a nearly rectangular area located just above the bed surface. The video recording system consisted of a progressive scan CCD video camera (Pulnix 6710) and a high-speed gated image intensifier (Hamamatsu Photonics, C4274) both synchronized to the laser pulses by means of a data acquisition/control unit. Frame-by-frame recording was accomplished at a sampling rate of 30 frames/s. The dimensions of the recorded area (0.285 wide, 0.21 m high digitized as 640x484 square pixels) resulted from a trade-off between the intensity of the fluorescence signal and the width of the window under scrutiny.

Materials

The fluidizing gas as well as the gas injected through the nozzle consisted of technical air at ambient conditions. Bed solids were glass beads (density: 2540 kg/m^3) of two different size ranges: 250-355 and 350-850 μm (average Sauter diameter: 277 μm and 530 μm, respectively) belonging to the Group B of the Geldart classification of powders. The incipient fluidization velocities (U_{mf}) of the bed materials were about 0.05 and 0.21 m/s. The settled bed height (H_{st}) was 0.32 m corresponding to a bed aspect ratio of 0.91 under static conditions. Acetone was used as gas tracer. Acetone has a light absorption wavelength band spanning between 210 and 310 nm with a maximum at about 270 nm. The fluorescence spectrum, typical of carbonyl compounds, spans over a broad wavelength region between 350 and 550 nm, with a maximum at about 420 nm. These features, together with the low toxicity and the large vapour pressure at room temperature, make acetone a suitable tracer for PLIF experiments at low temperatures.

Procedure

Experiments consisted of the injection of isolated traced bubbles in an incipiently fluidized bed. The fluidized state of the bed was monitored through the pressure drop across the bed. Data logging started immediately before the bubble was injected and lasted for a few seconds. The injected bubble diameter (D_b) was estimated on the basis of the pre-set volume of injected gas and of the extent of gas leakage according to a developed procedure (11) and was about 0.09 m. The influence of bed height above the bubble injection point on the hydrodynamics of bubble bursting was investigated changing the distance (H_{bs}) between the bubble injector and the bed surface. Image acquisition and post-processing were made by purposely written LabVIEW® procedures. A calibration procedure was developed to obtain quantitative acetone concentration data from PLIF measurements accounting for: i) the spatial profile of laser sheet intensity in the illuminated area; ii) the relationship between the fluorescence signal intensity and acetone concentration. The axial profile of the laser sheet intensity was recorded at the beginning and at the end of each test by focusing the laser sheet on a target uniformly covered by fluorescent compounds and located along the column axis. The fluorescence signal generated by the target was acquired by the video recording system and analyzed. The time-averaged axial profile of laser sheet intensity was normalized with reference to the local, the maximum and the minimum values of the fluorescence signal intensity along the height of the laser sheet. The relationship between the fluorescence signal intensity and acetone concentration was determined by

The 12th International Conference on Fluidization - New Horizons in Fluidization Engineering, Art. 55 [2007]

calibration. To this end, air at pre-set flow rate was continuously bubbled to saturation in liquid acetone maintained at 28°C. Acetone-saturated air was then mixed with a second air stream at a pre-set flow rate in order to obtain a mixture at the desired acetone concentration. The resulting stream was fed to the fluidization column by means of the bubble injection tube (for this purpose raised vertically with the exit nozzle inside the illuminated area). Acetone concentration was varied between 1 and 10 mol/m^3. Once background subtraction was made, a linear fit was established between fluorescence intensity and acetone concentration.

RESULTS

Phenomena associated with bursting of isolated bubbles at the surface of incipiently fluidized beds have been analyzed. The experimental campaign aimed at the characterization of the influence of two parameters, namely: a) the particle size of bed solids (fine, 277μm, versus coarse, 530μm, bed solids); b) the distance between the bubble injector and the bed surface (in the range between 0 and 0.20m). In all the experiments, the time at which the bubble approached the bed surface, identified by the incipient formation of a “dome” of bed solids, was taken as the origin t=0 of the time scale.

Influence of bed solids particle size

Fine bed material: Figure 2A reports a typical sequence of frames showing the raw fluorescence signal. Images were recorded immediately after the injection of an isolated bubble (calculated bubble diameter 0.09 m) in the bed of 250-355 μm glass beads at a distance H_{bs}=0.2 m from the bed surface. The bubble size and the distance of the injection nozzle from the bed surface are such that the sequential processes of bubble formation and bursting do not overlap nor interfere with each other. As the bubble approaches the bed surface, a “dome” of bed solids is raised. Bed solids are eventually ejected into the splash zone, and then they fall back to the bed surface. The observed bubble eruption patterns and gas flow structures are similar to those observed in previous experimental campaigns with planar laser induced scattering (PLLS) and fluorescence (PLIF) techniques on similar systems (9,11). In particular, the formation of two seeded gas regions is brought about by bubble bursting: a “nose” pocket and a toroidal vortex. The former becomes apparent immediately after dome formation (t=0.333 s) above the dome and is related to throughflow of a fraction of the seeded gas across the dome. As the remaining fraction of the seeded gas emerges at the bed surface with the bubble, it is squeezed away from the centreline (t=0.732 s) by the collapsing dome, contributing to the formation of the toroidal vortex (pocket). Altogether, the phenomenology of gas flow patterns appears to be dominated by the alternating piston-like motion of the ejected solids, responsible for the displacement of the seeded gas from the bubble trajectory and for imparting angular momentum to the toroidal vortex. The toroidal pocket rises at a nearly steady velocity (0.07 m/s, much smaller than the bubble rise velocity, 0.67m/s) and at the same time it enlarges by entraining gas from the mainstream (t=0.732 s, t=1.065 s, t=1.632 s).

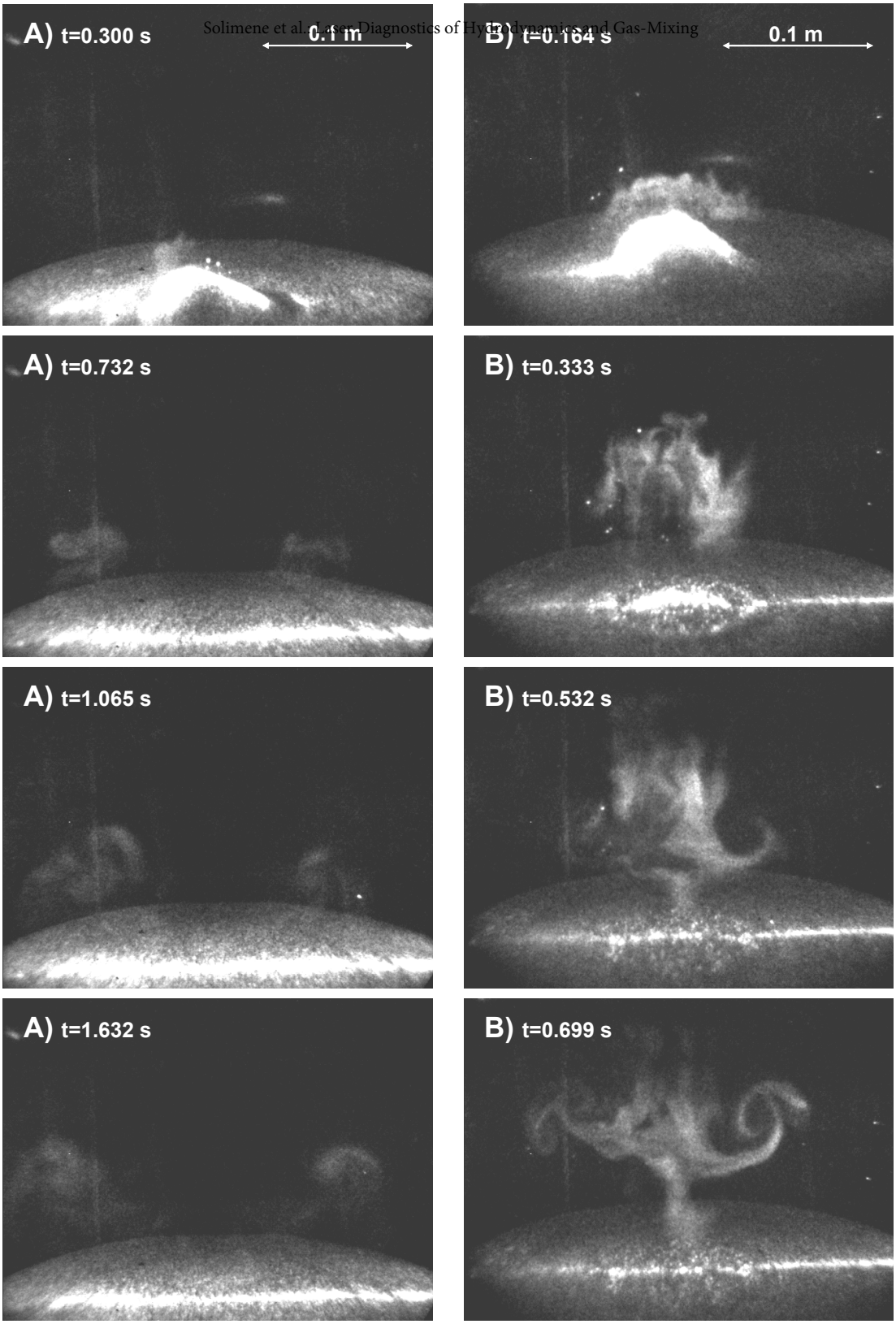

Fig. 2 Sequence of frames recorded after bubble injection into the fluidized bed (H_{bs} =0.2 m). A) 250-355 μm bed material, U=U_{mf}=0.05 m/s; B) 350-850 μm bed material, U=U_{mf}=0.21 m/s.

The 12th International Conference on Fluidization - New Horizons in Fluidization Engineering, Art. 55 [2007]

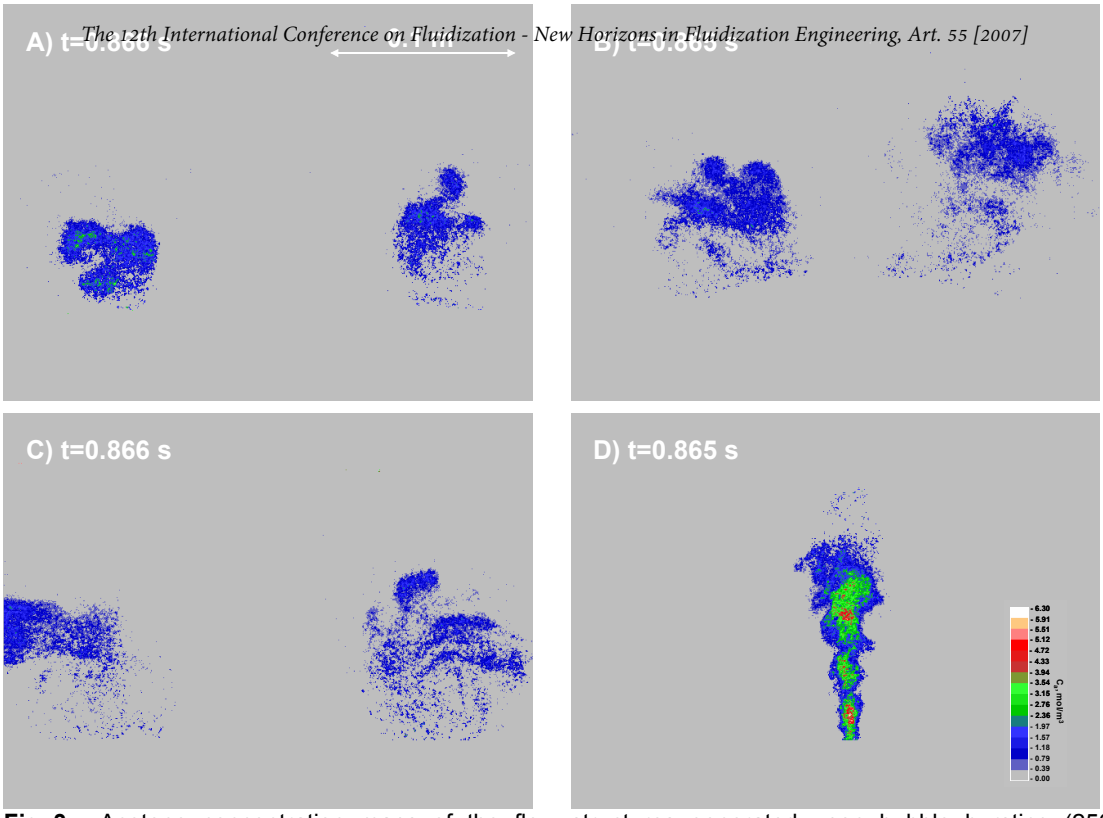

Fig. 3 Acetone concentration maps of the flow structures generated upon bubble bursting (250-355 μm bed material, $U=U_{mf}$=0.05 m/s). A) H_{bs} =0.2 m; B) H_{bs} =0.15 m; C) H_{bs} =0.05 m; D) H_{bs} =0 m.

The fine microstructure of the toroidal vortex is largely smoothed out due to the diffusive nature of the gas tracer, compared with similar results obtained with a non-diffusive solid tracer (11).

Coarse bed material: Figure 2B reports a sequence of frames for a typical test carried out under the same operating conditions of Fig.2A with bed material made of 350-850 μm glass beads. Though the general features of the phenomenology are somewhat preserved, major differences appear when hydrodynamic/mixing patterns observed with coarse bed material are compared with those observed with the bed of finer solids. The formation of a nose pocket (t=0.164 s) and a toroidal vortex are recorded also in this case (t=0.333 s, t=0.532 s, t=0.699 s). However a much larger amount of tracer gas is now found in the nose pocket, and a correspondingly smaller amount is entrained by the toroidal vortex. The toroidal vortex has a smaller diameter (defined as the distance between the center-of-mass of the two lobes) and a larger axial velocity (0.15 m/s) than the corresponding structure formed with the finer bed solids. Soon after bubble bursting, the nose pocket merges with the toroidal pocket, being dragged down and entrained by the latter. Altogether, bed particle size exerts a considerable influence on the flow structures associated with bubble bursting. All the noted differences should be related to the larger permeability of beds of coarser solids. This feature should determine: i) the larger throughflow of seeded gas across the dome during bubble eruption and, in turn, a bigger nose pocket; ii) a less effective drag exerted by the falling dome solids on the nose pocket; iii) a smaller momentum transfer between the collapsing dome and the emerging bubble gas which may result into smaller lateral displacement and larger axial velocity of the toroidal vortex.

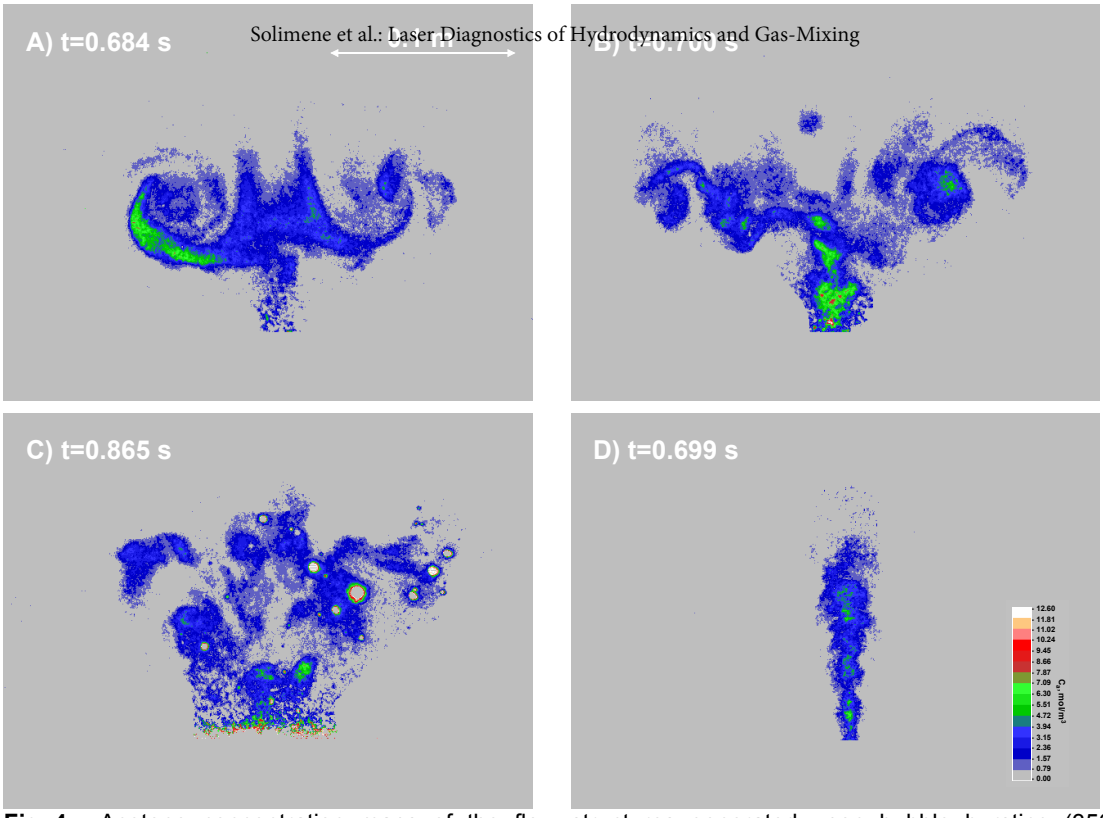

Fig. 4 Acetone concentration maps of the flow structures generated upon bubble bursting (350-850 μm bed material, $U=U_{mf}$=0.21 m/s). A) H_{bs} =0.2 m; B) H_{bs} =0.15 m; C) H_{bs} =0.05 m; D) H_{bs} =0 m.

Influence of bubble injection level.

Figures 3 and 4 report acetone concentration maps obtained by analyzing raw PLIF images obtained with fine and coarse bed material, respectively. Maps correspond to variable distances (H_{bs}) between the bubble injection level and the bed surface, varied between 0 and 0.20 m. The classical free-stream jet flow pattern is recorded when the injector is located flush to the bed surface (H_{bs}=0 m; Fig.3D; Fig.4D). On the contrary, the presence of even a shallow bed above the bubble injection point leads to the formation of a toroidal vortex (Fig.3A, 3B and 3C; Fig.4A, 4B and 4C). Changing H_{bs} (Fig.3A, 3B and 3C; Fig.4A, 4B and 4C) affects the gas flow pattern induced by bubble bursting. As H_{bs} is decreased, the vortex ring features: i) a larger cross sectional area (area of the lobes); ii) smaller values of acetone concentration. It is likely that these properties are all related to different ejection/fall back patterns of bed solids during bubble eruption as H_{bs} is varied. Decreasing H_{bs}, the dome size decreases and the mass of ejected solids is reduced accordingly. At the same time the ejected solids are characterized by larger velocity components directed along the column axis, a feature that is reflected by the higher levels above the bed surface to which bed solids can be launched. Moreover, the ejected solids appear looser and less “clustered” than the corresponding structures observed using deeper bubble injection levels. Altogether, these features are bound to affect the way bed solids interfere with gas emerging with the bubble during and after the burst, and the associated gas mixing.

CONCLUDING REMARKS

- A planar laser induced fluorescence imaging technique has been successfully employed to characterize hydrodynamic/mixing patterns associated with bubble bursting at the surface of incipiently fluidized beds.
- Bursting of isolated bubbles containing tracer gas gives rise to a composite flow structure: a nose pocket of seeded gas is generated due to gas throughflow across the dome; a toroidal vortex is generated by the interaction of the collapsing dome (acting similarly to a bluff body) with gas contained in the emerging bubble.
- The relative importance of the two basic structures (toroidal vortex, nose pocket) is critically dependent on the size of bed solids. The coarser the bed solids, the larger the fractional amount of seeding gas reporting to the nose pocket. Correspondingly, the amount reporting to the toroidal vortex is decreased.
- The patterns according to which the two basic structures (nose pocket, toroidal vortex) interact with the mainstream are very different. Extensive folding and stretching typical of the toroidal vortex should positively affect gas mixing, whereas the relatively unstretched/coherent motion of the nose pocket, together with its relatively small rise velocity compared with the bubble rise velocity, should be unfavourable to gas mixing. This argument, combined with the different partitioning of bubble gas between nose and toroidal pockets as a function of bed material, leads to the speculation that gas mixing in the splash zone should be more effective for beds of finer solids. This speculation is partly supported by analysis of tracer concentration maps obtained within the present study.
- The influence of bed depth above the bubble injection point has been investigated. Shallow beds as thin as 50mm are able to induce major departures of gas flow patterns from those typical of free-stream single-phase intermittent jets. The departure is due to the interaction of the emerging gas with solids in the dome. Solids ejection/fall back patterns are markedly influenced by the bubble injection level below the bed surface.

REFERENCES

1. Leckner, B., *Prog. Energy Combust. Sci.*, **24**, 31 (1998).
2. Scala, F. and Salatino, P., Chem. Engng. Sci., **57**, 1175 (2002).
3. Luecke, K., Hartge, E.-U. and Werther, J., *Int. J. Chem. Reactor Engng.*, **2** (2004).
4. Brink, A., Mueller, C. and Hupa, M., *the 19th International Conference on Fluidized Bed Combustion* Ed. Winter, F., paper 103, Vienna, Austria (2006).
5. Horio, M., Taki, A., Hsieh, Y. S. and Muchi, I., *Fluidization* Ed. Grace, R. J. and Matsen, M., 509, Plenum Press, New York (1980).
6. Pemberton, S. T. and Davidson, J. F., *Chem. Engng. Sci.*, **39**, 829 (1984).
7. Levy, Y. and Lockwood, F. C., *AIChE J.*, **29**, 889 (1983).
8. Caram, H. S., Efes, Z. and Levy, E. K., *AIChE Symp. Series*, **80** (234), 106 (1984).
9. Yorquez-Ramirez, M. I. and Duursma, G. R., *Chem. Engng Sci.*, **55**, 2055 (2000).
10. Yorquez-Ramirez, M. I. and Duursma, G. R. *Powder Technol.*, **116**, 76 (2001).
11. Solimene, R., Marzocchella, A., Ragucci, R. and Salatino, P., *Ind. Eng. Chem. Res.*, **43**, 5738 (2004).
12. Solimene, R., Marzocchella, A., Ragucci, R. and Salatino, P., *Chem. Engng. Sci.*, **62**, 94 (2007).
13. Solimene, R., Marzocchella, A., Passarelli, G. and Salatino, P., *A.I.Ch.E. J.*, **52**, 185 (2006).
14. Hamdullahpur, F. and MacKay, G. D. M. *AIChE J.*, **32**, 2047 (1986).